



HAL
open science

Can UAVs fill the gap between in situ surveys and satellites for habitat mapping?

Emilien Alvarez-Vanhard, Thomas Houet, Cendrine Mony, Lucie Lecoq,
Thomas Corpetti

► To cite this version:

Emilien Alvarez-Vanhard, Thomas Houet, Cendrine Mony, Lucie Lecoq, Thomas Corpetti. Can UAVs fill the gap between in situ surveys and satellites for habitat mapping?. *Remote Sensing of Environment*, 2020, 243, pp.111780. 10.1016/j.rse.2020.111780 . hal-02559702

HAL Id: hal-02559702

<https://hal.science/hal-02559702v1>

Submitted on 30 Apr 2020

HAL is a multi-disciplinary open access archive for the deposit and dissemination of scientific research documents, whether they are published or not. The documents may come from teaching and research institutions in France or abroad, or from public or private research centers.

L'archive ouverte pluridisciplinaire **HAL**, est destinée au dépôt et à la diffusion de documents scientifiques de niveau recherche, publiés ou non, émanant des établissements d'enseignement et de recherche français ou étrangers, des laboratoires publics ou privés.

1 **Can UAVs fill the gap between *in situ* surveys and satellites for habitat mapping ?**

2 Emilien Alvarez-Vanhard ^{1,3} *; Thomas Houet ^{1,3}; Cendrine Mony ^{2,3}; Lucie Lecoq ^{2,3}; Thomas

3 Corpetti ¹

4 ¹ CNRS UMR 6554 LETG, Université Rennes 2, Place du recteur Henri le Moal, 35000

5 Rennes, France

6 ² CNRS UMR 6553 ECOBIO, Université Rennes 1, Avenue Général Leclerc, 35000 Rennes,

7 France

8 ³ LTSER site "ZA Armorique"

9 * Corresponding author: alvarez_emilien@live.fr

10 **Abstract:**

11 Habitat mapping is an essential descriptor to monitor and manage natural or semi-natural
12 ecosystems. Habitats integrate both the environmental conditions and the related
13 biodiversity. However, it remains challenging to map certain habitats such as inland wetlands
14 due to spectral, spatial and temporal variability in the vegetation cover. Currently, no satellite
15 constellations optimize the spectral, spatial and temporal resolutions required to map
16 wetlands according to the habitats discriminated from *in situ* surveys. Our approach aims to
17 combine satellite and unmanned aerial vehicle (UAV) data to exceed their respective
18 limitations. Both data sources were combined through a spectral unmixing algorithm with the
19 hypothesis that endmembers from UAV data are pure enough to enhance plant community
20 abundances estimated from satellite data. The experiment was conducted on the regional
21 preserve of the Sougéal marsh, a wet grassland of 174 ha located upstream of the Mont-
22 Saint-Michel Bay. Two satellite data sources - Sentinel-2 and Pleiades - and three acquisition
23 periods - November 2017, April 2018 and May 2018 - were considered. A reference map of
24 plant community distribution was produced from UAV multitemporal data and floristic surveys
25 to validate the unmixing of satellite data. This study shows innovative results and
26 perspectives: while UAV can improve habitat discrimination, results vary among acquisition
27 periods and habitats. Results illustrate well the great potential of combined UAV and satellite
28 data but also demonstrate the influence of endmembers on the unmixing process and
29 technical limitations (e.g. spectral mismatches between sensors), which can be overcome
30 using domain adaptation.

31 **Keywords:** Unmanned Aerial Vehicle; sensor synergy; endmember; wetlands; spectral
32 unmixing; habitat mapping; LTSER Armorique

33 1. Introduction

34 Global changes caused by human activities are a major threat to ecosystems, leading to a
35 worldwide loss of biodiversity (Tilman et al., 2017), which calls for an assessment of the
36 conservation status of wetlands. Habitat mapping is essential to describe and monitor
37 ecosystems because habitats result from both environmental conditions and the ecosystem's
38 biodiversity (Lopez and Fennessy, 2002; Lu et al., 2015). Remote sensing (RS) has been
39 identified as a pertinent source of data to derive "essential biodiversity variables", (O'Connor
40 et al., 2015; Pereira et al., 2013), which can be used to characterize and monitor natural and
41 semi-natural ecosystems. They also help to discriminate ecosystem distributions at the
42 landscape scale, as well as habitat heterogeneity within these ecosystems (Alleaume et al.,
43 2018; Skidmore et al., 2015), providing useful indicators for supporting environmental
44 management of landscapes (Lu et al., 2015).

45 While habitats have been adequately mapped using RS for forest, heathland and grassland
46 ecosystems since the early 2000s (Corbane et al., 2015), mapping inland wetlands remains
47 challenging (Adam et al., 2010). Indeed, they encompass a wide diversity of ecosystems
48 driven by water stress, including humid and flooded grasslands. These ecosystems are of
49 particular interest since they provide many ecosystem services due to their hydrological,
50 ecological and biogeochemical functionalities (Costanza et al., 1997). They provide natural
51 and semi-natural habitats for rare fauna and flora and act as a refuge for wildlife diversity
52 (Denny, 1994). However, human land use leads to habitat degradation (Johnston et al.,
53 2009; Malekmohammadi and Jahanishakib, 2017), such as invasion by exotic or eutrophic
54 indigenous species, disturbances due to intensive agriculture or development of late-
55 successional vegetation stages due to land abandonment (Andrew and Ustin, 2009).
56 Detecting and monitoring habitat degradation in its early stages is of major importance for
57 land and biodiversity management (Walker and Smith, 1997). Accurately discriminating
58 habitats and mapping wet and flooded grasslands using optical RS is challenging (Adam et
59 al., 2010) since they exhibit high spectral and spatial variability in vegetation cover and
60 mixtures, which can become even more confused by local properties and processes (e.g.

61 underlying soil, hydrological regime, atmospheric water vapor, agricultural practices). It is
62 also difficult to define clear boundaries between habitats due to the spatio-temporal
63 dynamics of vegetation cover caused by seasonal and annual effects of climate and human
64 activities (Rapinel et al., 2019; Zlinszky et al., 2014). Although RS faces these challenges, it
65 remains the only way to exhaustively map large spatial areas that could not be covered by
66 *in-situ* surveys. Nevertheless, these surveys are crucial for training and validating RS results.
67 The accuracy of habitat maps depend strongly on the spectral, spatial and temporal
68 resolutions of RS imagery. First, the use of multispectral and hyperspectral data
69 demonstrates that as the spectral resolution increases, discrimination of habitats or species
70 becomes easier (Adam et al., 2010). Multispectral data allow for good discrimination (Sha et
71 al., 2008; Yang, 2007), although hyperspectral data provide more precise information about
72 biophysical and biochemical characteristics of habitats (Erudel et al., 2017; Silvestri et al.,
73 2003; Wang et al., 2007) or plants (Rebelo et al., 2018). However, hyperspectral data is only
74 currently available from airborne systems, which do not provide high frequency observations
75 over large areas except at high cost.. Second, high spatial resolution makes it possible to
76 extract features that describe textural or multi-scale characteristics, which allows for habitat
77 mapping at meter (Martínez-López et al., 2014) and sub-meter resolutions (Sawaya et al.,
78 2003; Szantoi et al., 2013). Very high spatial resolution (VHSR) sensors, such as Ikonos,
79 Quickbird or even Pleiades, however, have an associated cost that does not allow for
80 sufficiently frequent sampling to monitor habitats continuously over large areas (Guo et al.,
81 2017; Yang, 2007). Third, RS time series captures changes in vegetation spectra due to
82 phenology and hydrological regimes (Wang et al., 2012; Asner, 1998). Discrimination of
83 wetland and grassland has been improved by the use of the phenological variability in
84 reflectance (Ouyang et al., 2013; Rapinel et al., 2019; Gilmore et al., 2008; Schuster et al.,
85 2015). New satellite constellations such as Sentinel-2 provide high temporal frequency and
86 spectral richness, but their spatial resolution remains too low to discriminate small or patchy
87 habitat types effectively (Rapinel et al., 2019). Finally, no current satellite constellation offers
88 high-frequency temporal sampling with suitable high spatial and spectral resolutions;
89 however, optimizing the resolutions improved results (Rapinel et al., 2019). One way to

90 optimize resolutions is to combine several data sources, such as optical data from unmanned
91 aerial vehicles (UAV) and satellites.

92 Recent technological advances have made UAVs widely available, providing a new low-cost
93 RS data source with unrivalled properties (Anderson and Gaston, 2013). Despite their
94 inability to cover large areas, light UAVs can acquire VHSR multispectral data (Kaneko and
95 Nohara, 2014) at centimeter to decimeter spatial resolutions, which can be equivalent to pure
96 pixels. They are more flexible than traditional spaceborne or airborne sensors, allowing data
97 to be acquired at the same time as satellite data (Anderson and Gaston, 2013). Because of
98 this flexibility, we hypothesized that UAV data can be used to complement satellite data (e.g.
99 Pleiades, Sentinel-2) to improve mapping of wetland habitats. We assume that UAVs can
100 play an important role between field surveys and satellite data. Indeed, automatic mapping
101 depends on field surveys, which are expensive (Elzinga et al., 1998) and difficult to combine
102 with satellite imagery due to spatial and temporal topological errors (Karl et al., 2014; Zhang
103 et al., 2019) and, as mentioned, satellite resolutions that are too low. Thus, we examined
104 whether UAVs can fill the gap between *in situ* surveys and satellites.

105 Our study aimed to test spectral synergies between UAV and satellite data to map plant
106 communities, which were considered as habitat units. Reference spectra can be extracted
107 from UAV data to map habitats at a lower spatial resolution (satellite) using a spectral
108 unmixing approach (Roth et al., 2015). Unmixing allows the estimation of fractional
109 abundances of distinct habitat classes that have specific spectral signatures (i.e.
110 “endmembers”) (Keshava and Mustard, 2002). This approach has been applied to habitat
111 mapping (Hamada et al., 2013; Silvestri et al., 2003; Wang et al., 2007) and has the
112 advantage of considering plant communities as fuzzy sets (Bastin, 1997; Rocchini et al.,
113 2013), due to the variation in plant abundance along soil or altitudinal gradients. The main
114 limitation of unmixing processes is the need to select pure endmembers (or pixels), although
115 vegetation patterns have fine-grained spatial heterogeneity. Hamada et al. (2013) pointed out
116 that the purity of endmembers is the key to achieving good accuracy using a spectral
117 unmixing approach. This study assumes that the spatial resolution of UAV data helps in

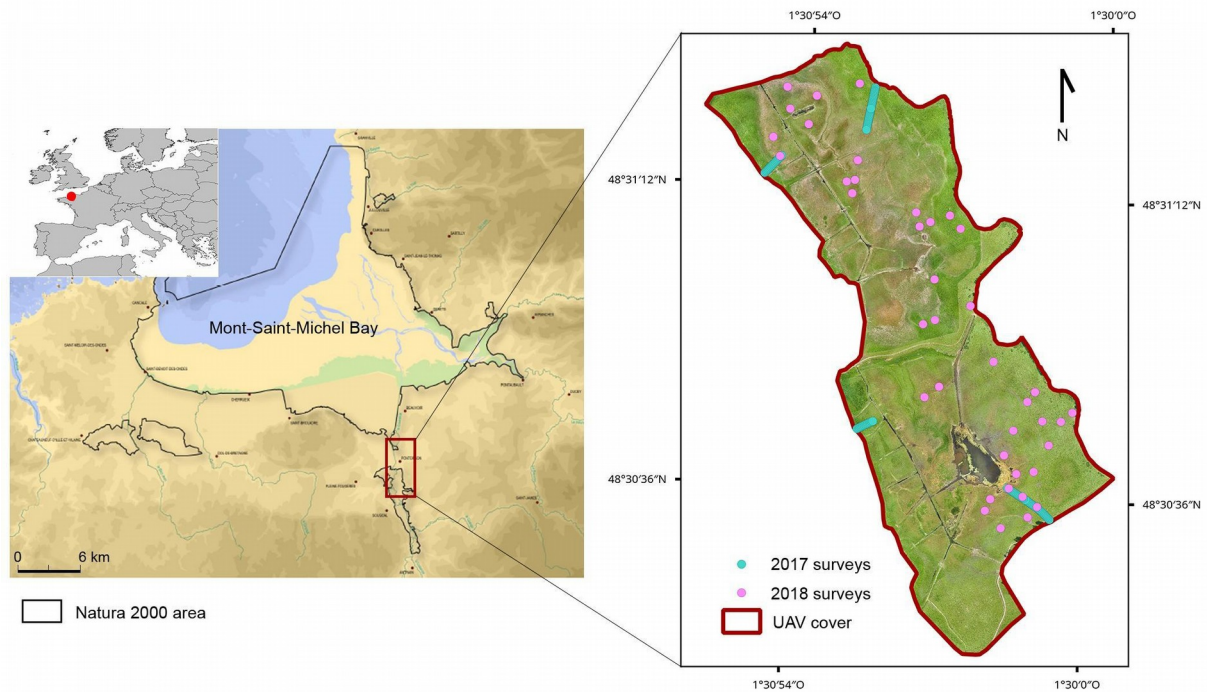
118 extracting pure endmembers.

119 To test these hypotheses, this study focused on the contribution of multispectral UAV data,
120 used along with satellite data, to map habitats using three RS datasets (UAV, Sentinel-2 and
121 Pleiades) and *in situ* floristic surveys. We focused specifically on analyzing the mosaic of
122 habitats of a flooded grassland in France. Their temporal (time series) and spatial (textural
123 information) resolutions were not considered.

124 **2. Materials**

125 *2.1. Study site*

126 The study was conducted in the Sougéal marsh (western France, 48.52° N, 1.53° W) which
127 is part of the LTSER site “Zone Atelier Armorique”. This site is a large flooded grassland of
128 174 ha located in the floodplain of the Couesnon River, upstream of Mont-Saint-Michel Bay
129 (Fig. 1). Due to its high conservation value, it has been included as a sub-site of the Natura
130 2000 “Baie du Mont Saint-Michel” site. It has been also labelled as a regional nature reserve.
131 It is regularly flooded from December to April, and managed through extensive mixed-grazing
132 of cows, horses and geese. It includes a network of shallow and stagnant channels, which
133 enables drainage of the site in spring. Plant assemblages are driven strongly by the flooding
134 gradient, encompassing different types of communities, from mesophilic to long-flooded
135 communities (assemblages described in Appendix A). The corresponding habitats are
136 identified using EUNIS typology (Ichter et al., 2014). Possible degradation of these habitats
137 has been detected at the site, particularly the spread of competitive eutrophic plant species
138 (e.g. *Urtica dioica*) and local trampling by cattle, which has created areas of bare soil.



140 Fig. 1. (left) Location of the Sougéal marsh study site on the Mont-Saint-Michel Bay Natura
 141 2000 site and (right) locations of floristic surveys in 2017 and 2018 on the orthophotograph
 142 acquired by UAV on 18 May 2018.

143 2.2. Field data

144 Plant assemblages were characterized by floristic surveys performed in May 2017 and May
 145 2018 (106 and 46 sampling plots, respectively; Fig. 1). For each plot of both surveys, we
 146 recorded all plant species and estimated their abundance as a percentage of cover in the
 147 plot. The first survey was performed by distributing plots along four transects parallel to the
 148 slope of the site to survey plant communities along the gradient of flooding duration. Plots
 149 measured 2×2 m and were located every 5 m along the transects. The second survey was
 150 performed to supplement the first. To include all possible variants of the communities
 151 identified at the site, plots were randomly placed in spatially homogeneous areas. These
 152 plots measured 50×50 cm.

153 2.3. Remotely sensed data

154 2.3.1. UAV data

155 UAV data were acquired for three dates (6 November 2017, 20 April 2018, 18 May 2018) to

156 provide a multi-season dataset providing information about the phenology and seasonality of
157 the habitats (Tomaselli et al., 2017). Two periods were selected to provide contrasting
158 phenologies: 1) before the winter floods (i.e. in November) and 2) after the winter floods,
159 starting in April, which corresponded to the flowering period and biomass peak, a key period
160 for identifying floristic patterns with spectral data (Deng et al., 2017; Feilhauer et al., 2013).
161 Although grazing had started by 18 May 2018, an exclusion zone had been established to
162 allow vegetation to grow. Spectral responses for a given community differed depending on
163 whether it was inside or outside this zone.

164 UAV data were acquired using an eBee+ (SenseFly, Cheseaux-sur-Lausanne, Switzerland),
165 a self-guided, lightweight (1.2 kg) and fixed-wing drone. Its mean duration is 40 minutes,
166 which allows it to cover up to 14 km² under fair meteorological conditions (low wind). Its
167 multispectral sensor (Sequoia, Parrot SA, Paris, France) acquired 1.2 megapixel images in
168 the green, red, red-edge and near infrared (NIR) bands (Fig. 2). It flew 148 m above the
169 ground, providing data at a resolution of 14.7 cm, which was resampled to 20 cm to provide
170 consistent spatial data for the study. The orthomosaics were generated for each
171 date/spectral band using Pix4dmapper software (Pix4D SA, Lausanne, Switzerland)
172 producing geometric error smaller than the pixel size (root mean square error (RMSE) =
173 0.048-0.154 m). Data were radiometrically corrected for optical instrument factors (e.g.
174 vignetting, spectral response) and differences in solar irradiance and angle, and calibrated
175 using a radiometric target to provide top-of-canopy (TOC) reflectance (Assmann et al., 2018).

176 2.3.2. Satellite data

177 Two types of multispectral satellite images were used: Sentinel-2 (ESA) and Pleiades
178 (Airbus) (Table 1). Satellite data were pre-processed at level 2A (i.e. orthorectified with
179 absolute ground reflectance values). Pleiades imaging was provided by the Centre National
180 d'Études Spatiales (CNES, the French spatial agency) KALIDEOS program at level 1C:
181 geometric corrections are accurate (< 0.7 m), while reflectance is retrieved using the
182 FLAASH algorithm (Cooley et al., 2002). Sentinel-2 images were pre-processed by the
183 CNES: radiometric corrections using the MACCS algorithm (Hagolle et al., 2015) and an

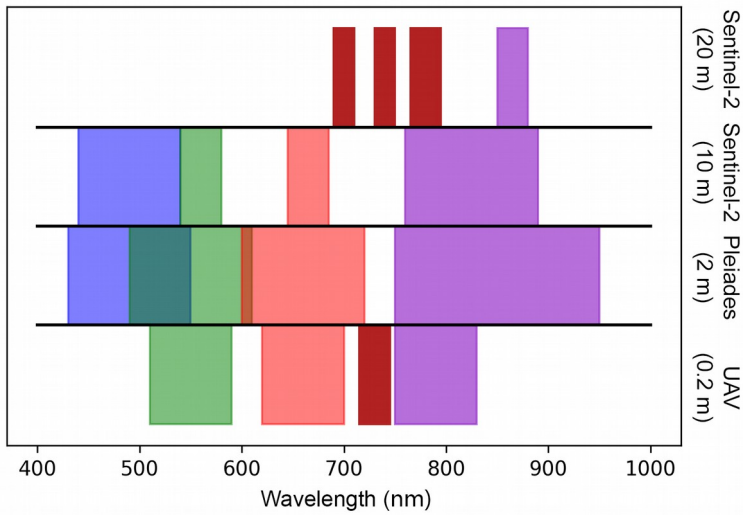
184 estimated positional error with an RMSE of 12.5 m (Dechoz et al., 2015) (i.e. a potential
 185 offset of > 50 pixels compared to UAV data). Pixels were adjusted empirically by shifting
 186 them to match ground-control points to minimize geometric mismatches between satellite
 187 and UAV data.

188 Table 1. Acquisition details for UAV, Sentinel-2 and Pleiades data.

Date	Sensor	Local time	Sensor incidence angle	Sensor azimuth angle	Solar zenith angle	Solar azimuth angle
6 Nov 2017	UAV	11:32:30	Near-nadir	/	64.181°	177.031°
6 Nov 2017	Pleiades	11:26:34	21.2762°	180.0429°	64.639°	173.643°
20 Apr	UAV	11:36:30	Near-nadir	/	36.281°	170.816°
2018						
19 Apr	Sentinel-2	10:56:19	Near-nadir	/	36.992°	166.341°
2018						
18 May	UAV	11:10:30	Near-nadir	/	29.548°	157.664°
2018						
20 May	Pleiades	11:25:34	17.7779°	180.0648°	29,298°	161.603°
2018						
19 May	Sentinel-2	10:56:19	Near-nadir	/	30.369°	151.244°
2018						

189

190 Spectral characteristics of the satellite and UAV images complemented each other (Fig. 2).
 191 All satellite and UAV images were acquired under clear-sky conditions with a maximum
 192 temporal mismatch between satellite and UAV acquisition of 2 days. Consequently, we
 193 assumed that the two sets of images did not differ significantly in spectral responses.

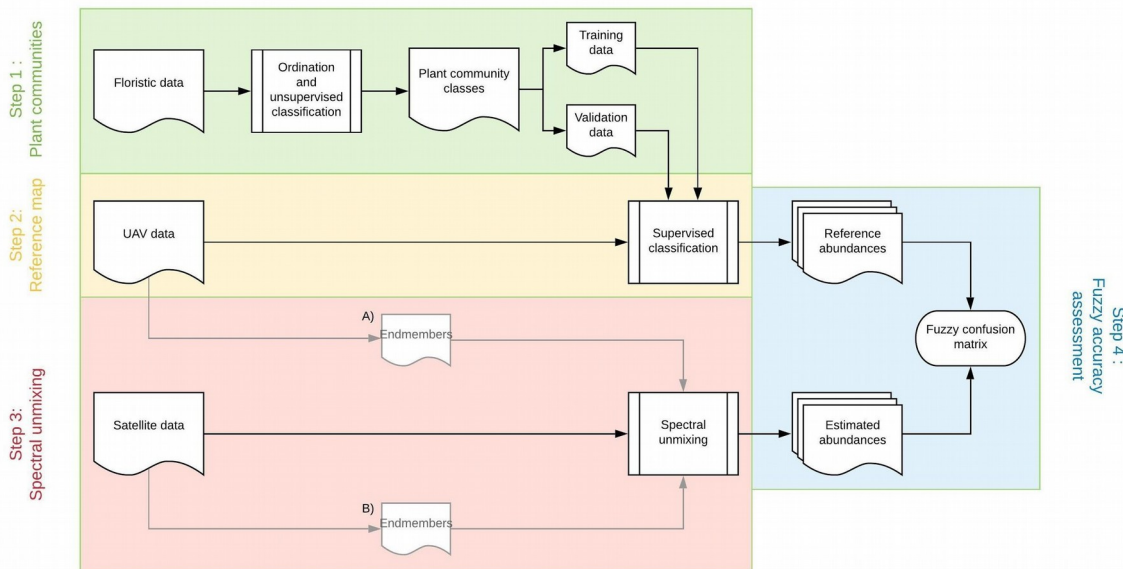


195 Fig. 2. Spectral (bandwidth) and spatial features of Sentinel-2, Pleiades and Sequoia (UAV)
 196 sensors.

197 **3. Methods**

198 The methodological workflow was stratified in four steps (Fig. 3), as described in the
 199 following subsections.

200



201 Fig. 3. The general workflow, composed of four steps: 1) unsupervised classification of
 202 floristic data, 2) supervised classification of multi-temporal UAV data to create a reference
 203 map, 3) estimation of plant community abundances by habitat based on two types of spectral
 204 unmixing (extraction of endmembers in (A) UAV imagery or (B) satellite imagery) and 4)

205 accuracy assessment.

206 3.1. Step 1: Unsupervised classification of floristic data

207 Plant groups were defined based on their floristic composition using correspondence
208 analysis (Greenacre, 2010) performed using the *FactoMineR* package of R software (R Core
209 Team, 2019). Groups were identified using hierarchical classification analysis based on the
210 coordinates of the sampled plots on the correspondence analysis axes. Four groups were
211 detected based on the plots sampled in 2017. Plots sampled in 2018 were projected as
212 supplementary individuals on the multivariate plots. Each sampling plot was assigned to a
213 group depending on its location in the multivariate plot. Seven plots that lay on the border
214 between two groups were removed from subsequent analysis. In total, floristic groups 1-4
215 contained 61, 19, 39 and 26 plots, respectively.

216 3.2. Step 2: Reference map: supervised classification of UAV data

217 The spatial distribution of plant communities was mapped using a supervised classification.
218 The entire UAV dataset, composed of spectral bands and three additional indices (NDVI,
219 NDVI-RE and NDWI; Gitelson and Merzlyak, 1994; Rouse et al., 1974; Xie et al., 2018) from
220 the three dates, was processed using one random forest (RF) model (Breiman, 2001). RF is
221 an ensemble classifier that generates multiple decision trees by randomly selecting a subset
222 of samples and variables (Belgiu and Drăguț, 2016). It is useful for RS data because it is
223 non-parametric and thus does not make assumptions about the distribution of the data,
224 which are rarely Gaussian. Moreover, it provides both hard and soft classifications that
225 correspond to probability maps of each class considered.

226 The RF classifier was set up to generate 300 trees. Then, the accuracy, choice of hyper-
227 parameters and robustness of RF classification was assessed by cross validation: the
228 sampling dataset from fields plots was divided into 10 subsets, each containing a nearly
229 equal number of each class. Each subset served successively as learning/validation data,
230 allowing the established model to be tested with 10 different sampling sets. The quality of the
231 classification was assessed using the Kappa index of agreement (KIA) and the overall
232 accuracy (OA). To optimize RF hyperparameters (maximum of features, maximum of leaf

233 nodes, ...), 20 values taken randomly have been tested for each subset for each subset and
234 the best one has been kept (see Appendix B). The RF and cross validation were performed
235 using the *scikit-learn* package in Python (Pedregosa et al., 2011).

236 3.3. Step 3: Estimation of abundances of plant communities

237 3.3.1.State-of-the-art: A priori assumption for analyzing spectral mixtures of plant 238 communities

239 Two steps are crucial in the unmixing process: selection of endmembers and estimation of
240 abundance. The first requires identifying the spectral signature of each endmember, which is
241 essential because spectral unmixing is entirely dependent on - and thus sensitive to - the
242 choice of endmembers (Tompkins et al., 1997). The flooding gradient creates fine-grained
243 spatial variability in plant communities, which makes endmember extraction challenging. To
244 include a wider range of variability, Multiple Endmember Spectral Mixing Analysis (MESMA)
245 was performed, in which each endmember is represented by several spectra (Roberts et al.,
246 1998). The second step - estimating the abundance matrix - uses the following equation (Eq.
247 1):

$$248 \quad X = E \times A \quad (\text{Eq. 1})$$

249 with X the signal received, E the endmember matrix and A the abundance matrix.

250 Then, MESMA attempts to minimize the residuals (Eq. 2).

$$251 \quad [L(X, EA) + P(E, A)] \quad (\text{Eq. 2})$$

252 with L a loss function (measuring the quality of the estimate) and P a penalty function (to
253 force the equation to achieve desired properties).

254 In this study, the spectral signal was a mixture of photons that interacted with different plant
255 species, soil and potentially water, which is assumed to be highly non-linear (Asner, 1998;
256 Borel and Gerstl, 1994; Roberts et al., 1993).

257 3.3.2.SAGA+ unmixing algorithm

258 The unmixing algorithm used to estimate abundances was SAGA+ (Nakhostin et al., 2016),

259 which is based on the geometric concept of finding the simplex that embeds data. The
260 simplex is calculated in a feature space associated with a kernel, which is useful when
261 analyzing non-linear mixtures. Each vertex of the simplex corresponds to an endmember.
262 Two constraints are imposed on the algorithm to avoid having all endmembers contribute to
263 the estimated solution: 1) the sparsity level (λ), which establishes the threshold below which
264 the abundance of an endmember becomes null, and 2) a maximum number of endmembers
265 per pixel (n_E).

266 3.4. Step 4: Accuracy assessment and optimization

267 The accuracy of satellite unmixing was assessed by calculating a fuzzy confusion matrix,
268 which is particularly suitable when using fuzzy classification (Binaghi et al., 1999). Unmixing
269 can indeed be viewed as a “soft” classifier in which the proportions of classes in each pixel is
270 extracted instead of a single class. Analyzing results with a fuzzy confusion matrix is thus
271 more consistent than analyzing only regression between abundances, since false positives
272 and false negatives are considered. The fuzzy confusion matrix was calculated by comparing
273 estimated abundances to reference abundances from RF probability maps. Like hard
274 classifications, this fuzzy matrix preserves the ability to locate errors and to derive the
275 following indicators from soft classifications: fuzzy OA (OA_f), fuzzy KIA (KIA_f), fuzzy
276 producer's accuracy (PA_f) and fuzzy user's accuracy (UA_f). Since the unmixing algorithm is
277 configurable, hyperparameter optimization (Kernel sigma, λ , n_E) was performed using KIA_f as
278 a quality criterion. The setting with the highest KIA_f was selected.

279 3.5. Experiments

280 3.5.1. Influence of acquisition features

281 The first experiment assessed the influence of the spatial/spectral resolutions of the satellite
282 sensor and the acquisition period on the spectral unmixing results. In May 2018, all types of
283 data were acquired almost simultaneously. Comparing results from Sentinel-2 and Pleiades
284 imagery while performing the same unmixing process would allow the respective influence of
285 the spectral and spatial resolution to be determined. The contribution of the spectral
286 resolution of Sentinel-2 was also tested by comparing the results obtained using its full

287 spectral resolution to those obtained with only the spectral bands similar to those in the UAV
 288 data. Since satellite images were acquired on three dates, the influence of the state of
 289 habitats (i.e. phenology, winter flooding) during a given period could be identified. Each
 290 satellite sensor was compared among the acquisition dates. To identify the tests performed,
 291 codes were established that combined the acquisition month (nov, apr, may), satellite sensor
 292 (pl, s2) and source of endmember data (sat, uav) (Table 2).

293 Table 2. Codes given to the unmixing processes tested

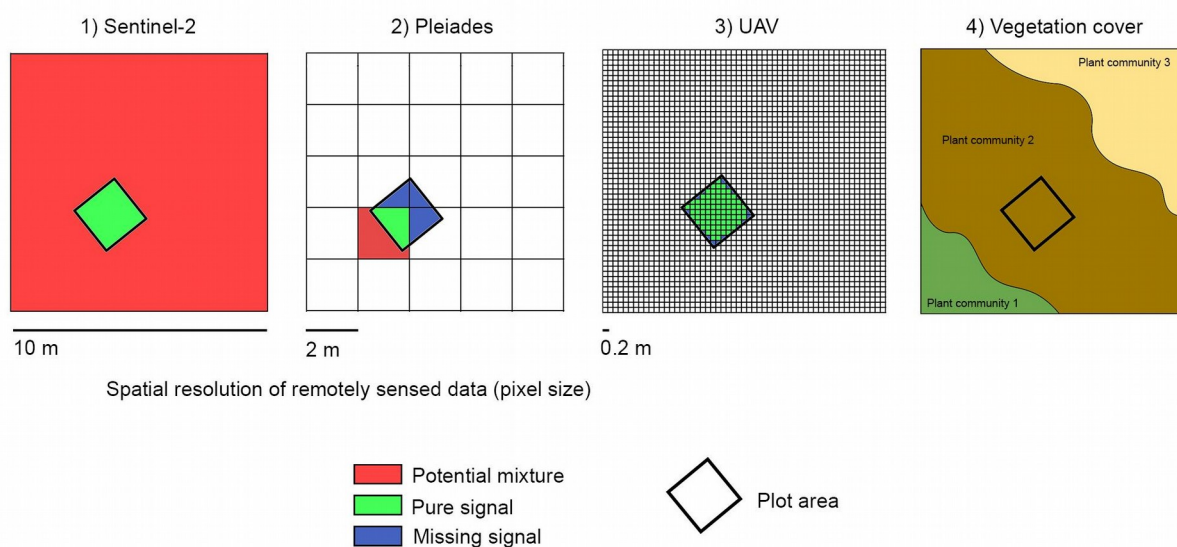
Date	Sensor	Images used to extract endmembers	Code
6 Nov 2017	Pleiades	Pleiades	nov-pl-sat
		UAV	nov-pl-uav
20 Apr 2018	Sentinel-2	Sentinel-2	apr-s2-sat
		UAV	apr-s2-uav
18 May 2018	Sentinel-2	Sentinel-2	may-s2-sat
		UAV	may-s2-uav
	Pleiades	Pleiades	may-pl-sat
		UAV	may-pl-uav

294

295 3.5.2. Influence of extracting endmembers from UAV vs. satellite data

296 The second experiment assessed the potential of UAV data to provide suitable endmembers
 297 for unmixing habitats. Two sources of endmembers were distinguished. The classic method
 298 consisted of extracting spectra from the satellite imagery that will be processed (case B, Fig.
 299 3). Their pixels are often assumed to be pure. The locations of sampling plots, acquired with
 300 a DGPS with a spatial accuracy of 2-3 cm, were used to extract endmembers. Since plots
 301 were separated by 5 m, however, a given pixel – especially in Sentinel-2 images (10 m
 302 spatial resolution) – may have covered two plots. If the two plots did not belong to the same
 303 habitat (i.e. the pixel covers two habitats), the corresponding spectrum was removed from
 304 the endmember matrix. Since sampling plots covered 2 × 2 m or less, even Pleiades images
 305 may have provided mixed spectral signatures, since the plots did not fit the image geometry
 306 perfectly (Fig. 4). The second method consisted of extracting endmembers from UAV images

307 (case A, Fig. 3), whose high spatial resolution (0.2 m) allowed us to assume that most pixels
 308 were pure (Fig. 4). Given the high spatial resolution of the UAV data, the number of spectra
 309 selected was too large to include all of them in the MESMA unmixing process; thus, the
 310 median spectral value was calculated for each sampling plot. This approach extracted
 311 endmembers of certain types and patches of vegetation that would not be detectable at lower
 312 resolutions because of their small size, such as *U. dioica* patches or bare soils, which are
 313 mainly long and narrow, corresponding to cattle pathways on the study site. The extracted
 314 endmembers are compared in Appendix C.
 315



316 Fig. 4. Influence of spatial resolution on the spectral response of survey areas. a) Sentinel-2
 317 resolution (10 m), b) Pleiades resolution (2 m), c) UAV resolution (0.2 m), d) Example of
 318 plant community distribution.

319 3.5.3. Influence of radiometric intercalibration

320 Combining optical RS data sources requires radiometric intercalibration. Each data source
 321 was processed for TOC reflectance. Despite these corrections, interoperability between
 322 sensors with different characteristics (e.g. spectral response, point spread function,
 323 instantaneous field of view) can produce errors (Teillet et al., 2007). To address this problem,
 324 the domain adaptation method was used (Tuia et al., 2016). This family of methods consists

325 of adapting data when one uses two sources with different characteristics (here, UAV and
326 satellite data) in order to compare them effectively. In practice, UAV data are transformed to
327 make them compatible with satellite data.

328 4. Results

329 4.1. Floristic typology

330 Four groups of plants were discriminated, which corresponded to plant assemblages
331 (Appendix A) along the flooding gradient (Appendix D):

- 332 • Group 1: mesophilic (M) communities (“E2.1 Permanent mesotrophic
333 pastures and aftermath-grazed meadows” in the EUNIS typology), dominated by
334 *Lolium perenne*, *Poa trivialis* and *Ranunculus repens*, with *Rumex obtusifolius*,
335 *R. crispus*, *Taraxacum officinale* and *Deschampsia cespitosa* as interstitial
336 species.
- 337 • Groups 2 and 3: meso-hygrophilic (MH) communities (“E3.4: Moist or wet
338 eutrophic and mesotrophic grassland” in the EUNIS typology), with group 2
339 dominated by *Alopecurus geniculatus* and *Poa trivialis*, with *Carex hirta*,
340 *Ranunculus sardous* and *Potentilla anserine* as interstitial species; and group 3
341 dominated by *Eleocharis acicularis* and *Agrostis stolonifera*, with *Ranunculus*
342 *flammula* as an interstitial species.
- 343 • Group 4: hygrophilic (H) communities (“E3.4: Moist or wet eutrophic and
344 mesotrophic grassland” in the EUNIS typology), dominated by *Glyceria fluitans*,
345 with *Veronica scutellata* and *Eleocharis palustris* as interstitial species.

346 4.2. Sub-pixel reference map

347 The supervised classification using RF and applied to multi-temporal UAV data discriminated
348 the four plant communities with an OA of 0.83 (± 0.07) and a KIA of 0.77 (± 0.10). The two
349 MH classes showed confusion between them (Appendix E), but once merged into a single
350 MH class, it was discriminated well from the two others (M and H). Once merged, its
351 classification had an OA of 0.90 (± 0.08) and a KIA of 0.85 (± 0.12). Analysis of the confusion
352 matrix (Table 3) showed little confusion between the classes; the lowest producer’s accuracy

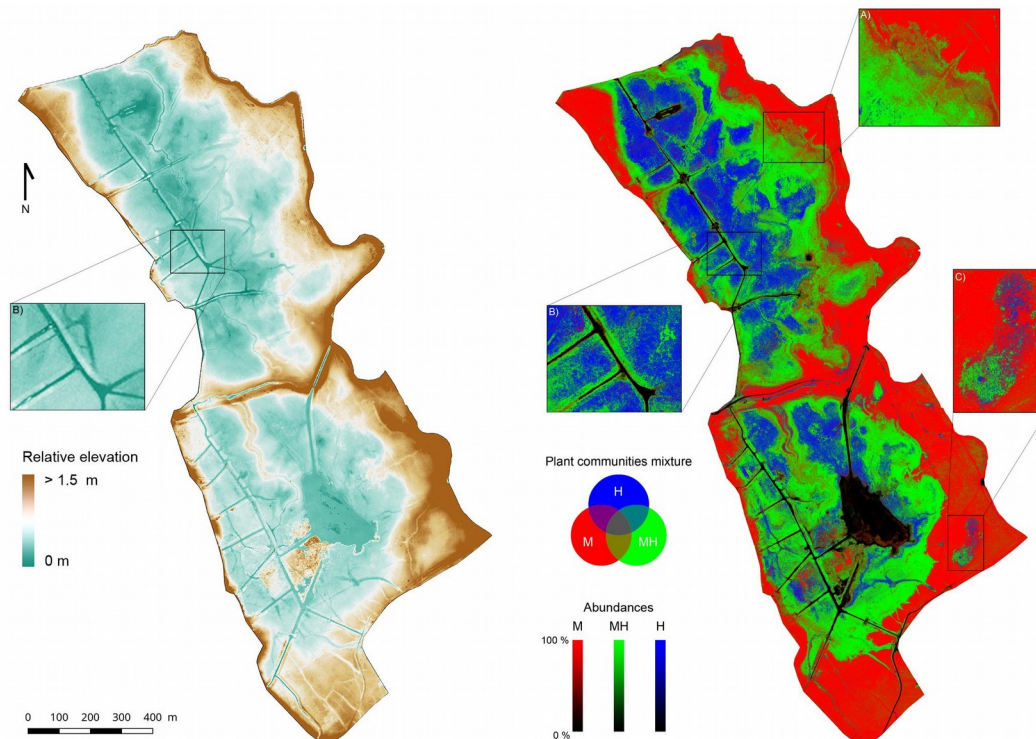
353 (PA) was 0.81 for class H. Nearly all commission and omission errors were between classes
 354 M and MH or H and MH. The three other classes considered (water, bare soils and *U. dioica*)
 355 were discriminated well, with few confusions. The relative importance of features is shown in
 356 Appendix F.

357 Table 3. Mean confusion matrix (%) between the random forest classification of three plant
 358 communities derived from UAV imagery (columns) and sampling plots (lines). Classes: M –
 359 mesophilic; MH – meso-hygrophilic; H – hygrophilic; BS - bare soils; Ud – *Urtica dioica* and
 360 W – water. PA: Producer’s accuracy, UA: User’s accuracy.

Class	Classification						PA	UA
	M	MH	H	Bs	U d	W		
R e f e r e n c e	M	31.9	4.4	0.2			0.93	0.87
	MH	2.1	38.8	1.8			0.87	0.91
	H		1.5	8.5			0.81	0.85
	Bs				2.8		0.98	0.98
	Ud	0.3				3.7	1.00	0.92
	W						3.9	0.90

361

362 Plant community abundances produced by the RF model (Fig. 5) highlight the complexity of
 363 the spatial distribution of habitats and their ecotones (i.e. transitions between two habitats).
 364 Some habitats were well discriminated at the southern end of the site, while the ecotones
 365 were fuzzier at the northern end, with interlaced habitats (Fig 5a). Habitat distribution
 366 logically depended on the topography. Drier locations in highest areas corresponded to M
 367 class, and vice-versa for H class. MH class was usually located between them. At the
 368 northern end of the site, small dikes on either side of channels with MH class on them were
 369 clearly identified (Fig 5b). Comparing the distribution of RF-classified communities to field
 370 observations confirmed the accuracy of the mapping, except for one artifact: a depression in
 371 the southeast corner of the study site that contained only H class was mapped instead as a
 372 pattern of all three classes (Fig. 5c).



374 *Fig. 5. Topography and plant communities of the Sougéal marsh. Left: digital surface model*
 375 *derived from UAV RGB data. Right: color composite of wet grassland plant communities in*
 376 *the Sougéal marsh derived from random forest classification of UAV imagery. Insets: a)*
 377 *ecotone, b) class MH on small dikes of channels and c) hygrophilic depression. Classes: M –*
 378 *mesophilic; MH – meso-hygrophilic; H – hygrophilic.*

379 4.3. Abundance estimation

380 4.3.1. Influence of satellite acquisition features

381 For May 2018, the best unmixing results were obtained for may-pl-sat ($OA_f = 0.68$ and $KIA_f =$
 382 0.53 ; Table 4). May-pl-sat was more effective than may-s2-sat, with a difference of $+0.10$
 383 KIA_f points. The two satellite sensors identified class M well, with a UA_f and PA_f exceeding
 384 0.70 for both (Fig. 7). However, Sentinel-2 did not detect class MH as well ($PA_f = 0.40$ and
 385 $UA_f = 0.64$) as Pleiades ($PA_f = 0.63$ and $UA_f = 0.71$). Both satellite sensors yielded poor
 386 results for bare soils, especially Sentinel-2, from whose data accurate endmembers for bare
 387 soils could not be extracted. Pleiades (Fig. 6g and 6h) clearly identified the channels, unlike
 388 Sentinel-2 (Fig. 6e and 6f). However, the latter provided higher abundances for each habitat
 389 with less plant community mixing – compared to those obtained from Pleiades (see Appendix
 390 G for details) – which is more consistent with field observations. Concerning Sentinel-2 data,

391 applying the same processes to a subset of satellite bands corresponding to those of the

392 UAV yielded identical results for both acquisition dates (apr-s2-sat and may-s2-sat).

393 Table 4. Unmixing results by endmember sources for each Sentinel-2 and Pleiades

394 acquisition. OA: overall accuracy, KIA: Kappa index of agreement, DA: domain adaptation.

Acquisition date	6 Nov 2017		20 Apr 2018		18 May 2018			
Sensor	Pleiades		Sentinel-2		Sentinel-2		Pleiades	
Score	OA _f	KIA _f	OA _f	KIA _f	OA _f	KIA _f	OA _f	KIA _f
Satellite endmembers	0.58	0.40	0.76	0.64	0.60	0.43	0.68	0.53
UAV endmembers	0.48	0.22	0.64	0.44	0.56	0.40	0.65	0.49
UAV endmembers (with DA)	0.58	0.38	0.71	0.57	0.65	0.51	0.65	0.51

395

396 Comparison of results highlighted the strong influence of acquisition date and solar zenith

397 angle: scores were higher for April and lower for November. For Pleiades, scores were

398 higher for May than for November (OA_f = 0.68 and 0.58, respectively). For Sentinel-2, scores

399 were higher for April than for May (OA_f = 0.76 and 0.6, respectively), while Pleiades yielded a

400 higher score than Sentinel-2 for May (OA_f = 0.65 and 0.60, respectively). Apr-s2-sat

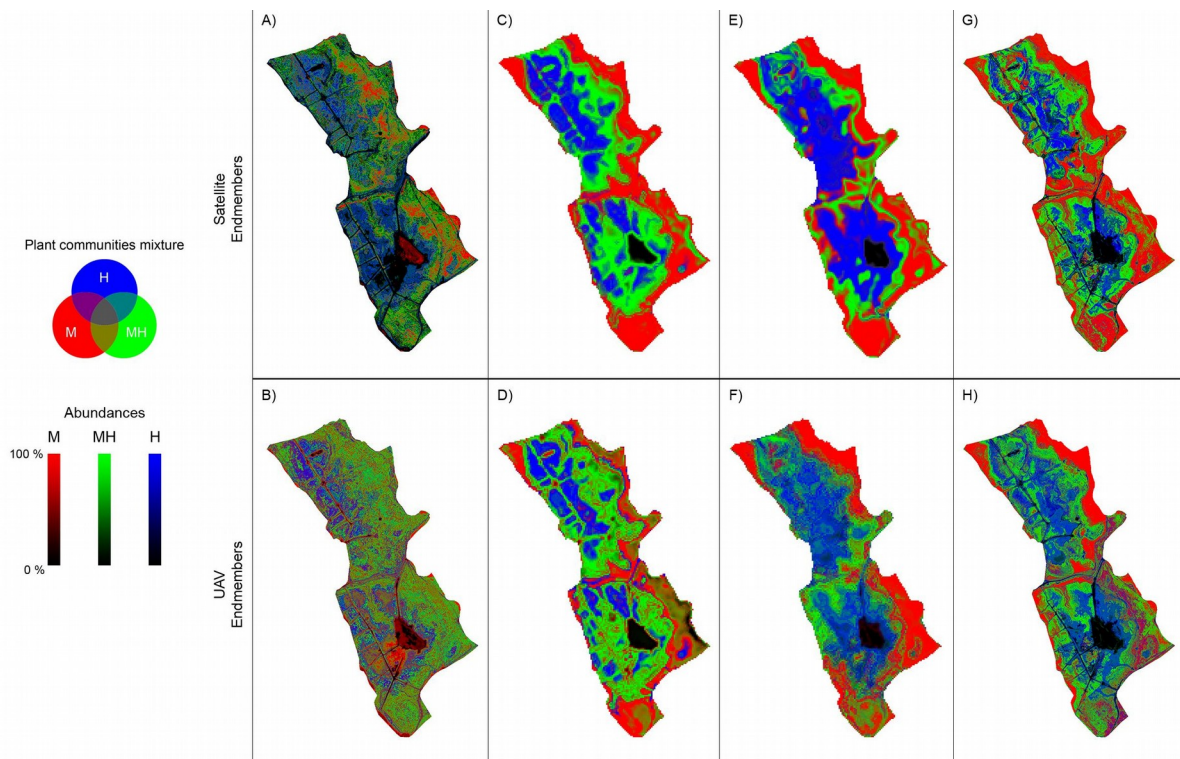
401 discriminated class M (PA_f = 0.80 and UA_f = 0.86) and class H class better (PA_f = 0.85 and

402 UA_f = 0.62). Estimated abundances for November showed strong confusion between plant

403 communities for nov-pl-sat (Fig 6a and 6b), while apr-s2-sat showed habitat patterns most

404 similar to the reference map. Estimates for May showed clear but different patterns for

405 classes H and MH.

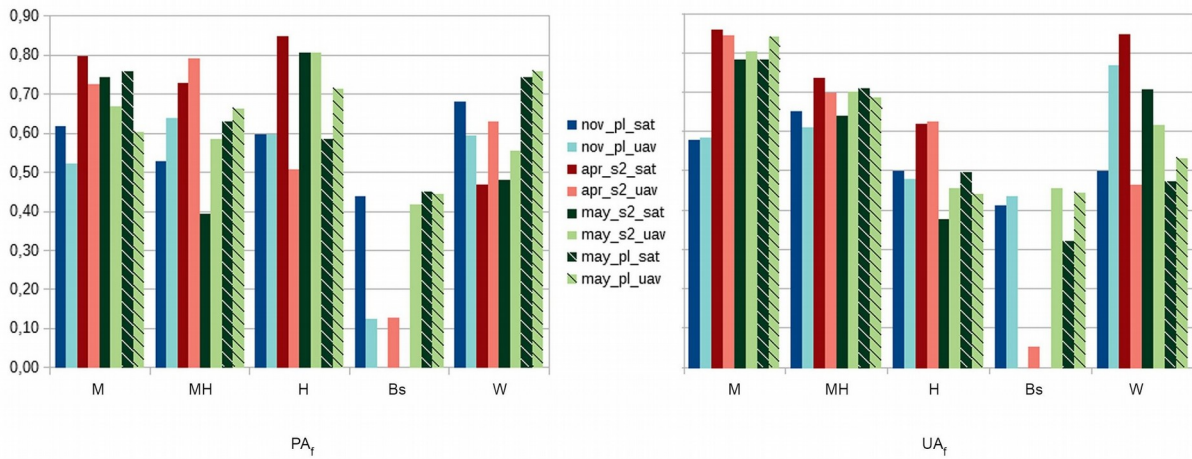


407 Fig. 6. Color composites of wet grassland plant communities in the Sougéal marsh derived
 408 from spectral unmixing of a) nov-pl-sat, b) nov-pl-uav, c) apr-s2-sat, d) apr-s2-uav, e) may-
 409 s2-sat, f) may-s2-uav, g) may-pl-sat, and h) may-pl-uav. See Table 2 for unmixing codes.

410 Classes: M – mesophilic; MH – meso-hygrophilic; H – hygrophilic.

411 4.3.2. Influence of endmembers extracted from UAV vs. satellite data

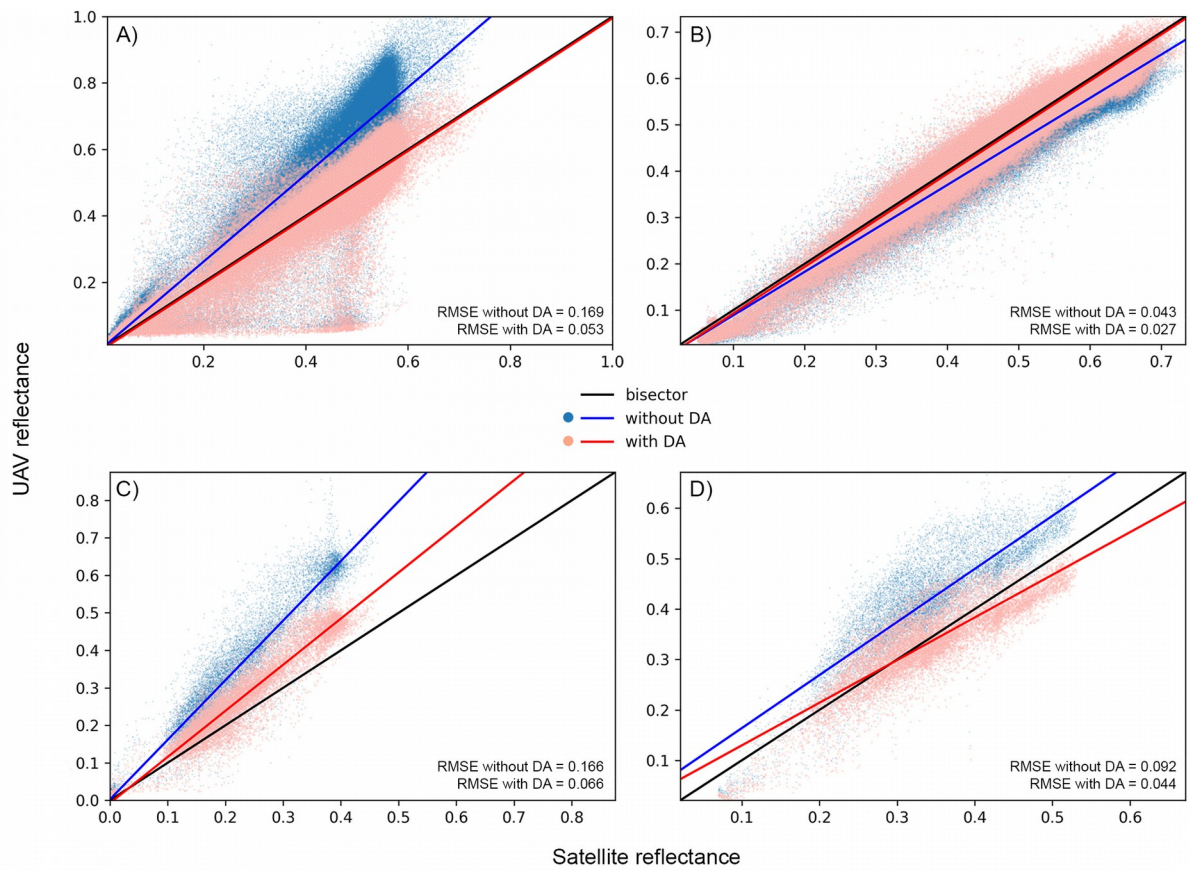
412 UAV-extracted endmembers rarely estimated abundances better than satellite-extracted
 413 endmembers (Table 4). May-s2-uav was the only experiment in which UAV-extracted
 414 endmembers had better results than satellite-extracted endmembers (+0.08 KIA_f points
 415 compared to may-s2-sat). The other experiments showed slightly lower OA_f or KIA_f scores
 416 when using UAV endmembers. UAV endmembers did not discriminate habitat classes as
 417 clearly as satellite ones (Fig. 6, darker hues). In certain cases, however, UAV endmembers
 418 always improved the PA_f for classes that were fuzzier (MH) or covered areas often smaller
 419 than satellites' pixel size (water, bare soils) (Fig. 7). For instance, may-pl-uav endmembers
 420 estimated class MH better (i.e. higher PA_f) than Sentinel-2 or Pleiades endmembers. UAV
 421 endmembers discriminated water better, especially may-pl-uav (PA_f = 0.76 and UA_f = 0.53).
 422 For bare soils, UAV-extracted estimates were similar to those extracted from Pleiades but
 423 always better than those extracted from Sentinel-2.



425 Fig. 7. Fuzzy producer's accuracy (PA_f) and user's accuracy (UA_f) by class and unmixing
 426 process. See Table 2 for unmixing codes. Classes: M – mesophilic; MH – meso-hygrophilic;
 427 H – hygrophilic; BS - bare soils; Ud – *Urtica dioica* and W – water.

428 4.3.3. Influence of radiometric intercalibration: domain adaptation

429 Domain adaptation adjusted the TOC reflectance values acquired with UAV to those of the
 430 satellite sensor, thus compensating for radiometric mismatches that remained after
 431 correcting each type of RS data (Fig. 8). Domain adaptation improved data intercalibration
 432 for all acquisition dates significantly: improvements were greater for November and April but
 433 less pronounced for May. Similarly, intercalibration of UAV data was better with Sentinel-2
 434 data (Fig. 8c and 8d) than with Pleiades data (Fig. 8a and 8b).



436 Fig. 8. Scatterplots of UAV vs. satellite reflectance with (red) and without (blue) domain
 437 adaptation (DA) for the near infrared spectral band: a) Pleiades on 6 November 2017, b)
 438 Pleiades on 20 May 2018, c) Sentinel-2 on 19 April 2018 and d) Sentinel-2 on 19 May 2018.

439 Using domain-adapted UAV endmembers improved all unmixing results, regardless of the
 440 date of acquisition (Table 5). The mean improvement was +0.09 KIA_f points, but
 441 improvement varied among dates (+0.01 to +0.16 KIA_f points, +0.01 to +0.09 OA_f points).

442 The accuracy of the results was strongly correlated with the quality of the intercalibration of
 443 the data sources.

444 Table 5. Improvements in spectral calibration of UAV data (RMSE) and unmixing results with
 445 UAV endmembers (overall accuracy (OA_f) and Kappa index of agreement (KIA_f)) between
 446 applying and not applying the domain adaptation method.

Data source and date	ΔOA_f	ΔKIA_f	$\Delta RMSE$ (NIR)
Pleiades (6 Nov 2017)	+0.09	+0.16	-0.116
Pleiades (18 May 2018)	+0.01	+0.01	-0.016

Sentinel-2 (20 Apr 2018)	+0.06	+0.09	-0.096
Sentinel-2 (19 May 2018)	+0.09	+0.11	-0.048

447

448 **5. Discussion**

449 Broadly, this study demonstrates that UAVs show great potential to fill the gap between *in*
450 *situ* surveys and satellite imagery for providing and improving RS essential biodiversity
451 variables. The spectral unmixing approach allowed for estimation of mixed habitats and
452 overcame the spatial resolution constraint of satellite sensors by providing subpixel
453 information. MESMA has already demonstrated its ability to integrate the variability in
454 heterogeneous plant classes but at lower spatial resolutions (Li et al., 2005; Michishita et al.,
455 2012; Rosso et al., 2005). When used to map natural or semi-natural habitats, it enables 1)
456 discrimination of community patterns with a grain size smaller than the spatial resolution of
457 the sensor (Roth et al., 2015) and 2) representation of ecotones between two habitats (Hill et
458 al., 2007).

459 *5.1. Endmember effectiveness in spectral, spatial and temporal dimensions*

460 Endmember selection remains a challenging task that can be controversial. The dataset
461 used made it possible to evaluate influences of spectral, spatial and temporal dimensions in
462 this crucial step of habitat mapping in flooded and humid grasslands in a temperate oceanic
463 climate.

464 First, spectral resolution is known to be essential for discriminating wetland plant
465 communities (Adam et al., 2010), and it is an important feature when analyzing the spectral
466 mixture (Bioucas-Dias et al., 2012). Surprisingly, however, we found that including all
467 Sentinel-2 spectral bands did not improve analysis of the spectral mixture for the Sougéal
468 marsh. The increased spectral resolution from the additional bands (6 red-edge, NIR and
469 mid-infrared bands at 20 m) may not have compensated for the decrease in the spatial
470 resolution. This study also shows that spectral intercalibration of RS data is crucial to perform
471 unmixing of satellite data with endmembers from a different source. Even though data were
472 radiometrically corrected to produce TOC reflectance, mismatches in spectral values
473 remained between UAV and satellite data, especially in the green and NIR bands (Appendix

474 H). Overestimation of spectral values by the UAV's Sequoia multispectral sensor is
475 suspected because its grassland reflectances exceeded 0.6 in the NIR. Domain adaptation
476 overcame these problems, although testing the quality and interoperability of the sensor is
477 required for future scientific studies.

478 Second, most endmembers extracted from high-spatial-resolution imagery yielded better
479 results. Pleiades, with a spatial resolution 5 times as high as that of Sentinel-2, yielded better
480 results in May 2018. One can assume that the VHSR images of Pleiades make it possible to
481 extract endmembers that are not influenced by potential class mixtures (Roth et al., 2015).
482 Higher-spatial-resolution UAV data can also help extract a pure spectral signature, but also
483 one that could be too specific, depending on the grain size of plant community patterns.
484 Nonetheless, UAV endmembers always improved discrimination of the meso-hygrophilic
485 class, which is floristically more heterogeneous because of variations in flooding throughout
486 the year (Bonis, 2014). This result suggests that endmembers from VHSR data are more
487 suitable for heterogeneous classes, for which acquisition of pure pixels is more complicated.
488 In future studies, VHSR data could be used to purify endmember spectral bands by
489 identifying and eliminating endmembers influenced by the background (Bian et al., 2016; Ma
490 et al., 2015).

491 *Finally, this study strengthens the ability of RS data to discriminate plant communities better*
492 *during specific periods. Like Rapinel et al. (2019), acquiring images in early spring (April),*
493 *near the biomass peak and flowering of plants, appears to help discriminate plant*
494 *communities greatly (Feilhauer et al., 2013). The grain size of plant community patterns may*
495 *vary among periods depending on the hydrological regime (Corriale et al., 2013; Todd et al.,*
496 *2010). The differences in spatial patterns identified between the periods studied (e.g.*
497 *hygrophilic habitat in April and May) were likely due to confusion caused by certain species*
498 *common to several habitats but not present in all vegetation belts, due to the flooding*
499 *gradient over time, which causes spatial and temporal phenological shifts. Depending on*
500 *land use, vegetation types and vegetation dynamics (i.e. during the acquisition period),*
501 *selection of endmembers can be even more subtle than expected. Hence, integrating multi-*

502 *temporal endmembers when a phenological gradient is present is an interesting prospect*
503 *(Dudley et al., 2015).*

504 5.2. *Synergies among In situ, UAV and satellite data*

505 UAV technology shows great potential for successfully mapping habitats of the Sougéal
506 marsh at a spatial resolution never achieved before (20 cm). VHSR imagery played two
507 major roles in this study: clarifying and validating satellite data. First, UAV data were used to
508 extract “pure” endmembers to clarify satellite data using the unmixing algorithm (Schaaf et
509 al., 2011), which estimated plant community abundances. Second, combining UAV data with *in*
510 *situ* surveys provided a spatially exhaustive ground truth to assess these estimated
511 abundances. However, the accuracy of the reference map can be questioned, because
512 spatial and temporal phenological shifts could contribute to a failure to discriminate habitats
513 properly. For instance, ecotones can represent one of these shifts, ultimately belonging to
514 one habitat rather than a mixture of two. Moreover, grazing activities (May-November) are
515 likely to influence spectral signatures of plant communities and may lead to local
516 misclassifications. Producing a monthly time series of UAV data, for instance, would help
517 discriminate these habitats by monitoring floods and vegetation phenology.

518 This study focused on spectral complementarities between UAV and satellite data. Spatial
519 and temporal complementarities still need to be explored. Indeed, UAV data provide high-
520 resolution textural (vegetation patterns or heterogeneity) and topographical information that
521 can be useful for habitat mapping. These spatial features can complement spectral
522 information to differentiate complex environments in which vegetation communities have a
523 strong spectral similarity (Zhao and Du, 2016). Object-oriented approaches that include
524 texture information allow for multi-scale analyses (Moffett and Gorelick, 2013; Tuxen and
525 Kelly, 2008) and could be used with a convolutional neural network to automatically extract
526 multi-scale spatial features. This method has proven to be even more effective for wetland
527 mapping (Mahdianpari et al., 2018; Rezaee et al., 2018) than traditional classifiers such as
528 RF. Finally, an interesting perspective for combining UAV and satellite data is spatio-
529 temporal fusion, which allows for modeling of high-resolution images using two data sources,
530 one at high spatial resolution and the other at high temporal resolution (Chen et al., 2015).

531 5.3. Remote sensing: a proxy of the state of biodiversity

532 Using UAVs for RS provides good discrimination or estimation of wetland habitats at level 3
533 of the EUNIS typology on the Sougéal marsh, despite grazing, which prevents vegetation
534 from developing fully. Classifying species groups into plant communities is based essentially
535 on the presence of certain species that characterize the habitat; however, the abundances of
536 all of its constituent species contributes most to the spectral signature of the plant
537 community. The spectral signal acquired does not make it possible to identify the typical
538 species of the community, which may have low abundance. On the contrary, the dominant
539 species in the community contribute the most to the spectral signature. Nonetheless, this
540 study demonstrates that UAV data have great potential to enhance discrimination of
541 herbaceous habitats in humid grasslands at a fine level of nomenclature (typological
542 resolution below EUNIS level 3), whether combined with satellite data or not.

543 Habitat mapping has been recognized for more than 40 years as a good proxy of
544 biodiversity. Beyond its assessment of habitat types, this study also demonstrates that some
545 indices of conservation status can be estimated in wetland habitats, such as the proliferation
546 of eutrophic species (*U. dioica*) or the occurrence of local disturbances due to intensive
547 grazing (i.e. bare soils). This opens new avenues for using UAV technology in a broader
548 objective of analyzing the ecosystem functioning related to habitat presence, distribution and
549 ecological status.

550 6. Conclusion

551 This study evaluated the utility of UAV data to fill the gap between *in situ* survey and satellite
552 data for habitat mapping. The main results showed that UAVs have great potential for habitat
553 mapping: they are flexible (allowing data to be acquired at the same time as satellite data),
554 can map habitats on small areas (up to ca. 100 ha) effectively and provide training
555 (endmember) and validation (habitat class) data for unmixing high-temporal-resolution
556 satellite multispectral data, such as Sentinel-2 (10 m) or Pleiades (2.4 m). Fuzzy
557 classifications of mesophilic, meso-hygrophilic and hygrophilic communities were produced
558 with good to reasonable accuracy when combining UAV endmembers and satellite data,
559 although the study revealed some technical limitations and the challenge of mapping of these

560 habitats. For the former, although it is necessary to intercalibrate sensors to increase the
561 accuracy of habitat maps, domain adaptation can overcome spectral mismatches. For the
562 latter, some acquisition periods were more suitable than others. The influence of climate,
563 hydrological regimes and land use (here, grazing) may lead to spatial and temporal shifts in
564 habitat phenology, making it difficult to discriminate boundaries of flooded grassland habitats
565 accurately. However, UAV data contribute to early detection of invasive species or land
566 degradation whose mean area remains smaller than the spatial resolution of satellite images.
567 Futur work is needed to benefit fully from potential synergies between satellite and UAV data
568 for environmental applications. Although focused only on spectral synergies, this study
569 identified promising improvements by combining spatial and temporal characteristics.

570 **Acknowledgements**

571 This study was supported by public funds (Région Bretagne) received in the framework of
572 the emerging research project (PER) coordinated by "Groupement Bretagne Télédétection"
573 (BreTel), the ANR project MATS ([ANR-18-CE23-0006](#)) and from the European Regional
574 Development Fund (ERDF) under the umbrella of INTERREG Atlantic Area
575 (EAPA_261/2016) "Improving the management of Atlantic Landscapes: accounting for
576 biodiversity and ecosystem services (ALICE)". Data provisioning was supported by the
577 LTSER "Zone Atelier Armorique", the KALIDEOS Bretagne satellite acquisition program
578 supported by the CNES and by public funds received in the framework of GEOSUD, a
579 project (ANR-10-EQPX-20) of the "Investissements d'Avenir" program managed by the
580 French National Research Agency and the DroneSat Project supported by the University of
581 Rennes 2.

582 **References**

583 Adam, E., Mutanga, O., Rugege, D., 2010. Multispectral and hyperspectral remote sensing
584 for identification and mapping of wetland vegetation: a review. *Wetl. Ecol. Manag.* 18,
585 281–296. <https://doi.org/10.1007/s11273-009-9169-z>
586 Alleaume, S., Dusseux, P., Thierion, V., Commagnac, L., Laventure, S., Lang, M., Féret, J.-
587 B., Hubert-Moy, L., Luque, S., 2018. A generic remote sensing approach to derive

588 operational essential biodiversity variables (EBVs) for conservation planning.
589 *Methods Ecol. Evol.* 9, 1822–1836. <https://doi.org/10.1111/2041-210X.13033>

590 Anderson, K., Gaston, K.J., 2013. Lightweight unmanned aerial vehicles will revolutionize
591 spatial ecology. *Front. Ecol. Environ.* 11, 138–146. <https://doi.org/10.1890/120150>

592 Andrew, M.E., Ustin, S.L., 2009. Habitat suitability modelling of an invasive plant with
593 advanced remote sensing data. *Divers. Distrib.* 15, 627–640.
594 <https://doi.org/10.1111/j.1472-4642.2009.00568.x>

595 Asner, G.P., 1998. Biophysical and Biochemical Sources of Variability in Canopy
596 Reflectance. *Remote Sens. Environ.* 64, 234–253. [https://doi.org/10.1016/S0034-](https://doi.org/10.1016/S0034-4257(98)00014-5)
597 [4257\(98\)00014-5](https://doi.org/10.1016/S0034-4257(98)00014-5)

598 Assmann, J.J., Kerby, J.T., Cunliffe, A.M., Myers-Smith, I.H., 2018. Vegetation monitoring
599 using multispectral sensors - best practices and lessons learned from high latitudes.
600 *bioRxiv* 334730. <https://doi.org/10.1101/334730>

601 Bastin, L., 1997. Comparison of fuzzy c-means classification, linear mixture modelling and
602 MLC probabilities as tools for unmixing coarse pixels. *Int. J. Remote Sens.* 18, 3629–
603 3648. <https://doi.org/10.1080/014311697216847>

604 Belgiu, M., Drăguț, L., 2016. Random forest in remote sensing: A review of applications and
605 future directions. *ISPRS J. Photogramm. Remote Sens.* 114, 24–31.
606 <https://doi.org/10.1016/j.isprsjprs.2016.01.011>

607 Bian, J., Li, A., Zhang, Z., Zhao, W., Lei, G., Xia, H., Tan, J., 2016. Grassland fractional
608 vegetation cover monitoring using the composited HJ-1A/B time series images and
609 unmanned aerial vehicles: A case study in Zoige wetland, China, in: 2016 IEEE
610 International Geoscience and Remote Sensing Symposium (IGARSS). Presented at
611 the 2016 IEEE International Geoscience and Remote Sensing Symposium (IGARSS),
612 pp. 7192–7195. <https://doi.org/10.1109/IGARSS.2016.7730876>

613 Binaghi, E., Brivio, P.A., Ghezzi, P., Rampini, A., 1999. A fuzzy set-based accuracy
614 assessment of soft classification. *Pattern Recognit. Lett.* 20, 935–948. [https://doi.org/](https://doi.org/10.1016/S0167-8655(99)00061-6)
615 [10.1016/S0167-8655\(99\)00061-6](https://doi.org/10.1016/S0167-8655(99)00061-6)

616 Bioucas-Dias, J.M., Plaza, A., Dobigeon, N., Parente, M., Du, Q., Gader, P., Chanussot, J.,
617 2012. Hyperspectral Unmixing Overview: Geometrical, Statistical, and Sparse
618 Regression-Based Approaches. ArXiv12026294 Phys. Stat.

619 Bonis, A., 2014. Hydropériode des zones humides : un enjeu décisif pour la structure des
620 communautés végétales et leur diversité. Lavoisier.

621 Borel, C.C., Gerstl, S.A.W., 1994. Nonlinear spectral mixing models for vegetative and soil
622 surfaces. Remote Sens. Environ. 47, 403–416. [https://doi.org/10.1016/0034-](https://doi.org/10.1016/0034-4257(94)90107-4)
623 [4257\(94\)90107-4](https://doi.org/10.1016/0034-4257(94)90107-4)

624 Breiman, L., 2001. Random Forests. Mach. Learn. 45, 5–32.
625 <https://doi.org/10.1023/A:1010933404324>

626 Chen, B., Huang, B., Xu, B., 2015. Comparison of Spatiotemporal Fusion Models: A Review.
627 Remote Sens. 7, 1798–1835. <https://doi.org/10.3390/rs70201798>

628 Cooley, T., Anderson, G.P., Felde, G.W., Hoke, M.L., Ratkowski, A.J., Chetwynd, J.H.,
629 Gardner, J.A., Adler-Golden, S.M., Matthew, M.W., Berk, A., Bernstein, L.S., Acharya,
630 P.K., Miller, D., Lewis, P., 2002. FLAASH, a MODTRAN4-based atmospheric
631 correction algorithm, its application and validation, in: IEEE International Geoscience
632 and Remote Sensing Symposium. Presented at the IEEE International Geoscience
633 and Remote Sensing Symposium, pp. 1414–1418 vol.3.
634 <https://doi.org/10.1109/IGARSS.2002.1026134>

635 Corbane, C., Lang, S., Pipkins, K., Alleaume, S., Deshayes, M., García Millán, V.E.,
636 Strasser, T., Vanden Borre, J., Toon, S., Michael, F., 2015. Remote sensing for
637 mapping natural habitats and their conservation status – New opportunities and
638 challenges. Int. J. Appl. Earth Obs. Geoinformation, Special Issue on Earth
639 observation for habitat mapping and biodiversity monitoring 37, 7–16.
640 <https://doi.org/10.1016/j.jag.2014.11.005>

641 Corriale, M.J., Picca, P.I., di Francescantonio, D., 2013. Seasonal variation of plant
642 communities and their environments along a topographic gradient in the Iberá
643 wetland, ancient Paraná floodplain, Argentina. Phytocoenologia 53–69.
644 <https://doi.org/10.1127/0340-269X/2013/0043-0539>

645 Costanza, R., d'Arge, R., Groot, R. de, Farber, S., GrasSo, M., Hannon, B., Limburg, K.,
646 Naeem, S., O'Neill, R.V., Paruelo, J., Raskin, R.G., Sutton, P., Belt, M. van den,
647 1997. The value of the world's ecosystem services and natural capital. *Nature* 387,
648 253. <https://doi.org/10.1038/387253a0>

649 Dechoz, C., Poulain, V., Massera, S., Languille, F., Greslou, D., de Lussy, F., Gaudel, A.,
650 L'Helguen, C., Picard, C., Trémas, T., 2015. Sentinel 2 global reference image, in:
651 Bruzzone, L. (Ed.), . p. 96430A. <https://doi.org/10.1117/12.2195046>

652 Deng, C., Li, C., Zhu, Z., Lin, W., Xi, L., 2017. Subpixel urban impervious surface mapping:
653 the impact of input Landsat images. *ISPRS J. Photogramm. Remote Sens.* 133, 89–
654 103. <https://doi.org/10.1016/j.isprsjprs.2017.09.015>

655 Denny, P., 1994. Biodiversity and wetlands. *Wetl. Ecol. Manag.* 3, 55–611.
656 <https://doi.org/10.1007/BF00177296>

657 Dudley, K.L., Dennison, P.E., Roth, K.L., Roberts, D.A., Coates, A.R., 2015. A multi-temporal
658 spectral library approach for mapping vegetation species across spatial and temporal
659 phenological gradients. *Remote Sens. Environ., Special Issue on the Hyperspectral*
660 *Infrared Imager (HyspIRI)* 167, 121–134. <https://doi.org/10.1016/j.rse.2015.05.004>

661 Elzinga, C., Salzer, D., Willoughby, J., 1998. *Measuring & Monitoring Plant Populations*. US
662 Bur. Land Manag. Pap.

663 Erudel, T., Fabre, S., Houet, T., Mazier, F., Briottet, X., 2017. Criteria Comparison for
664 Classifying Peatland Vegetation Types Using In Situ Hyperspectral Measurements.
665 *Remote Sens.* 9, pages 1-62. <https://doi.org/10.3390/rs9070748>

666 Feilhauer, H., Thonfeld, F., Faude, U., He, K.S., Rocchini, D., Schmidlein, S., 2013.
667 Assessing floristic composition with multispectral sensors—A comparison based on
668 monotemporal and multiseasonal field spectra. *Int. J. Appl. Earth Obs.*
669 *Geoinformation* 21, 218–229. <https://doi.org/10.1016/j.jag.2012.09.002>

670 Gilmore, M.S., Wilson, E.H., Barrett, N., Civco, D.L., Prisloe, S., Hurd, J.D., Chadwick, C.,
671 2008. Integrating multi-temporal spectral and structural information to map wetland
672 vegetation in a lower Connecticut River tidal marsh. *Remote Sens. Environ.* 112,
673 4048–4060. <https://doi.org/10.1016/j.rse.2008.05.020>

674 Gitelson, A., Merzlyak, M.N., 1994. Spectral Reflectance Changes Associated with Autumn
675 Senescence of *Aesculus hippocastanum* L. and *Acer platanoides* L. Leaves. Spectral
676 Features and Relation to Chlorophyll Estimation. *J. Plant Physiol.* 143, 286–292.
677 [https://doi.org/10.1016/S0176-1617\(11\)81633-0](https://doi.org/10.1016/S0176-1617(11)81633-0)

678 Guo, M., Li, J., Sheng, C., Xu, J., Wu, L., 2017. A Review of Wetland Remote Sensing.
679 *Sensors* 17, 777. <https://doi.org/10.3390/s17040777>

680 Greenacre, M., 2010. Correspondence analysis of raw data. *Ecology* 91, 958–963.
681 <https://doi.org/10.1890/09-0239.1>

682 Hagolle, O., Huc, M., Villa Pascual, D., Dedieu, G., 2015. A Multi-Temporal and Multi-
683 Spectral Method to Estimate Aerosol Optical Thickness over Land, for the
684 Atmospheric Correction of FormoSat-2, LandSat, VEN μ S and Sentinel-2 Images.
685 *Remote Sens.* 7, 2668–2691. <https://doi.org/10.3390/rs70302668>

686 Hamada, Y., Stow, D.A., Roberts, D.A., Franklin, J., Kyriakidis, P.C., 2013. Assessing and
687 monitoring semi-arid shrublands using object-based image analysis and multiple
688 endmember spectral mixture analysis. *Environ. Monit. Assess.* 185, 3173–3190.
689 <https://doi.org/10.1007/s10661-012-2781-z>

690 Hill, R.A., Granica, K., Smith, G.M., Schardt, M., 2007. Representation of an alpine treeline
691 ecotone in SPOT 5 HRG data. *Remote Sens. Environ., ForestSAT Special Issue* 110,
692 458–467. <https://doi.org/10.1016/j.rse.2006.11.031>

693 Ichter, J., Evans, D., Richard, D., Poncet, L., Spyropoulou, R., Pereira Martins, I., European
694 Environment Agency, Museum national d'Histoire naturelle (MNHN), 2014. Terrestrial
695 habitat mapping in Europe: an overview. Publications Office, Luxembourg.

696 Johnston, C.A., Zedler, J.B., Tulbure, M.G., Frieswyk, C.B., Bedford, B.L., Vaccaro, L., 2009.
697 A unifying approach for evaluating the condition of wetland plant communities and
698 identifying related stressors. *Ecol. Appl.* 19, 1739–1757. [https://doi.org/10.1890/08-](https://doi.org/10.1890/08-1290.1)
699 [1290.1](https://doi.org/10.1890/08-1290.1)

700 Karl, J.W., Taylor, J., Bobo, M., 2014. A double-sampling approach to deriving training and
701 validation data for remotely-sensed vegetation products. *Int. J. Remote Sens.* 35,
702 1936–1955. <https://doi.org/10.1080/01431161.2014.880820>

703 2014. Review of Effective Vegetation Mapping Using the UAV (Unmanned Aerial
704 Vehicle) Method. *J. Geogr. Inf. Syst.* 06, 733–742.
705 <https://doi.org/10.4236/jgis.2014.66060>

706 Keshava, N., Mustard, J.F., 2002. Spectral unmixing. *IEEE Signal Process. Mag.* 19, 44–57.
707 <https://doi.org/10.1109/79.974727>

708 Li, L., Ustin, S.L., Lay, M., 2005. Application of multiple endmember spectral mixture analysis
709 (MESMA) to AVIRIS imagery for coastal salt marsh mapping: a case study in China
710 Camp, CA, USA. *Int. J. Remote Sens.* 26, 5193–5207.
711 <https://doi.org/10.1080/01431160500218911>

712 Lopez, R.D., Fennessy, M.S., 2002. Testing the Floristic Quality Assessment Index as an
713 Indicator of Wetland Condition. *Ecol. Appl.* 12, 487–497. [https://doi.org/10.1890/1051-
714 0761\(2002\)012\[0487:TTFQAI\]2.0.CO;2](https://doi.org/10.1890/1051-0761(2002)012[0487:TTFQAI]2.0.CO;2)

715 Lu, Y., Wang, R., Zhang, Y., Su, H., Wang, P., Jenkins, A., Ferrier, R.C., Bailey, M., Squire,
716 G., 2015. Ecosystem health towards sustainability. *Ecosyst. Health Sustain.* 1, 1–15.
717 <https://doi.org/10.1890/EHS14-0013.1>

718 Ma, L., Zhou, Y., Chen, J., Cao, X., Chen, X., 2015. Estimation of Fractional Vegetation
719 Cover in Semiarid Areas by Integrating Endmember Reflectance Purification Into
720 Nonlinear Spectral Mixture Analysis. *IEEE Geosci. Remote Sens. Lett.* 12, 1175–
721 1179. <https://doi.org/10.1109/LGRS.2014.2385816>

722 Mahdianpari, M., Salehi, B., Rezaee, M., Mohammadimanesh, F., Zhang, Y., 2018. Very
723 Deep Convolutional Neural Networks for Complex Land Cover Mapping Using
724 Multispectral Remote Sensing Imagery. *Remote Sens.* 10, 1119.
725 <https://doi.org/10.3390/rs10071119>

726 Malekmohammadi, B., Jahanishakib, F., 2017. Vulnerability assessment of wetland
727 landscape ecosystem services using driver-pressure-state-impact-response (DPSIR)
728 model. *Ecol. Indic.* 82, 293–303. <https://doi.org/10.1016/j.ecolind.2017.06.060>

729 Martínez-López, J., Carreño, M.F., Palazón-Ferrando, J.A., Martínez-Fernández, J., Esteve,
730 M.A., 2014. Remote sensing of plant communities as a tool for assessing the
731 condition of semiarid Mediterranean saline wetlands in agricultural catchments. *Int. J.*

732 Appl. Earth Obs. Geoinformation 26, 193–204.
733 <https://doi.org/10.1016/j.jag.2013.07.005>

734 Michishita, R., Gong, P., Xu, B., 2012. Spectral mixture analysis for bi-sensor wetland
735 mapping using Landsat TM and Terra MODIS data. *Int. J. Remote Sens.* 33, 3373–
736 3401. <https://doi.org/10.1080/01431161.2011.611185>

737 Moffett, K.B., Gorelick, S.M., 2013. Distinguishing wetland vegetation and channel features
738 with object-based image segmentation. *Int. J. Remote Sens.* 34, 1332–1354.
739 <https://doi.org/10.1080/01431161.2012.718463>

740 Nakhostin, S., Clenet, H., Corpetti, T., Courty, N., 2016. Joint Anomaly Detection and
741 Spectral Unmixing for Planetary Hyperspectral Images. *IEEE Trans. Geosci. Remote*
742 *Sens.* 54, 6879–6894. <https://doi.org/10.1109/TGRS.2016.2586188>

743 O'Connor, B., Secades, C., Penner, J., Sonnenschein, R., Skidmore, A., Burgess, N.D.,
744 Hutton, J.M., 2015. Earth observation as a tool for tracking progress towards the Aichi
745 Biodiversity Targets. *Remote Sens. Ecol. Conserv.* 1, 19–28.
746 <https://doi.org/10.1002/rse2.4>

747 Ouyang, Z.-T., Gao, Y., Xie, X., Guo, H.-Q., Zhang, T.-T., Zhao, B., 2013. Spectral
748 Discrimination of the Invasive Plant *Spartina alterniflora* at Multiple Phenological
749 Stages in a Saltmarsh Wetland. *PloS One* 8, e67315.
750 <https://doi.org/10.1371/journal.pone.0067315>

751 Pedregosa, F., Varoquaux, G., Gramfort, A., Michel, V., Thirion, B., Grisel, O., Blondel, M.,
752 Prettenhofer, P., Weiss, R., Dubourg, V., Vanderplas, J., Passos, A., Cournapeau, D.,
753 Brucher, M., Perrot, M., Duchesnay, É., 2011. Scikit-learn: Machine Learning in
754 Python. *J. Mach. Learn. Res.* 12, 2825–2830.

755 Pereira, H.M., Ferrier, S., Walters, M., Geller, G.N., Jongman, R.H.G., Scholes, R.J., Bruford,
756 M.W., Brummitt, N., Butchart, S.H.M., Cardoso, A.C., Coops, N.C., Dulloo, E., Faith,
757 D.P., Freyhof, J., Gregory, R.D., Heip, C., Höft, R., Hurtt, G., Jetz, W., Karp, D.S.,
758 McGeoch, M.A., Obura, D., Onoda, Y., Pettorelli, N., Reyers, B., Sayre, R.,
759 Scharlemann, J.P.W., Stuart, S.N., Turak, E., Walpole, M., Wegmann, M., 2013.

760 Essential Biodiversity Variables. *Science* 339, 277–278.
761 <https://doi.org/10.1126/science.1229931>

762 Pix4D. 2019. Support website. Available from <https://support.pix4d.com/hc/en-us> [accessed
763 18 October 2019]

764 Rapinel, S., Mony, C., Lecoq, L., Clément, B., Thomas, A., Hubert-Moy, L., 2019. Evaluation
765 of Sentinel-2 time-series for mapping floodplain grassland plant communities. *Remote*
766 *Sens. Environ.* 223, 115–129. <https://doi.org/10.1016/j.rse.2019.01.018>

767 Rebelo, A.J., Somers, B., Esler, K.J., Meire, P., 2018. Can wetland plant functional groups
768 be spectrally discriminated? *Remote Sens. Environ.* 210, 25–34.
769 <https://doi.org/10.1016/j.rse.2018.02.031>

770 Rezaee, M., Mahdianpari, M., Zhang, Y., Salehi, B., 2018. Deep Convolutional Neural
771 Network for Complex Wetland Classification Using Optical Remote Sensing Imagery.
772 *IEEE J. Sel. Top. Appl. Earth Obs. Remote Sens.* 11, 3030–3039.
773 <https://doi.org/10.1109/JSTARS.2018.2846178>

Roberts, D.A., Smith, M.O., Adams, J.B., 1993. Green vegetation, nonphotosynthetic
vegetation, and soils in AVIRIS data. *Remote Sens. Environ., Airbone Imaging*
Spectrometry 44, 255–269. [https://doi.org/10.1016/0034-4257\(93\)90020-X](https://doi.org/10.1016/0034-4257(93)90020-X)

774 Roberts, D.A., Gardner, M., Church, R., Ustin, S., Scheer, G., Green, R.O., 1998. Mapping
775 Chaparral in the Santa Monica Mountains Using Multiple Endmember Spectral
776 Mixture Models. *Remote Sens. Environ.* 65, 267–279. [https://doi.org/10.1016/S0034-](https://doi.org/10.1016/S0034-4257(98)00037-6)
777 [4257\(98\)00037-6](https://doi.org/10.1016/S0034-4257(98)00037-6)

778 Rocchini, D., Foody, G.M., Nagendra, H., Ricotta, C., Anand, M., He, K.S., Amici, V.,
779 Kleinschmit, B., Förster, M., Schmidlein, S., Feilhauer, H., Ghisla, A., Metz, M.,
780 Neteler, M., 2013. Uncertainty in ecosystem mapping by remote sensing. *Comput.*
781 *Geosci., Benchmark problems, datasets and methodologies for the computational*
782 *geosciences* 50, 128–135. <https://doi.org/10.1016/j.cageo.2012.05.022>

783 Rosso, P.H., Ustin, S.L., Hastings, A., 2005. Mapping marshland vegetation of San
784 Francisco Bay, California, using hyperspectral data. *Int. J. Remote Sens.* 26, 5169–
785 5191. <https://doi.org/10.1080/01431160500218770>

786 Roth, K.L., Roberts, D.A., Dennison, P.E., Peterson, S.H., Alonzo, M., 2015. The impact of
787 spatial resolution on the classification of plant species and functional types within
788 imaging spectrometer data. *Remote Sens. Environ.* 171, 45–57.
789 <https://doi.org/10.1016/j.rse.2015.10.004>

790 Rouse, J.W., Jr., Haas, R.H., Schell, J.A., Deering, D.W., 1974. Monitoring Vegetation
791 Systems in the Great Plains with ERTS. *NASA Spec. Publ.* 351, 309.

792 Sawaya, K.E., Olmanson, L.G., Heinert, N.J., Brezonik, P.L., Bauer, M.E., 2003. Extending
793 satellite remote sensing to local scales: land and water resource monitoring using
794 high-resolution imagery. *Remote Sens. Environ., IKONOS Fine Spatial Resolution
795 Land Observation* 88, 144–156. <https://doi.org/10.1016/j.rse.2003.04.006>

796 Schaaf, A.N., Dennison, P.E., Fryer, G.K., Roth, K.L., Roberts, D.A., 2011. Mapping Plant
797 Functional Types at Multiple Spatial Resolutions Using Imaging Spectrometer Data.
798 *GIScience Remote Sens.* 48, 324–344. <https://doi.org/10.2747/1548-1603.48.3.324>

799 Schuster, C., Schmidt, T., Conrad, C., Kleinschmit, B., Förster, M., 2015. Grassland habitat
800 mapping by intra-annual time series analysis – Comparison of RapidEye and
801 TerraSAR-X satellite data. *Int. J. Appl. Earth Obs. Geoinformation* 34, 25–34.
802 <https://doi.org/10.1016/j.jag.2014.06.004>

803 Sha, Z., Bai, Y., Xie, Y., Yu, M., Zhang, L., 2008. Using a hybrid fuzzy classifier (HFC) to
804 map typical grassland vegetation in Xilin River Basin, Inner Mongolia, China. *Int. J.
805 Remote Sens.* 29, 2317–2337. <https://doi.org/10.1080/01431160701408436>

806 Silvestri, S., Marani, M., Marani, A., 2003. Hyperspectral remote sensing of salt marsh
807 vegetation, morphology and soil topography. *Phys. Chem. Earth Parts ABC,
808 Applications of Quantitative Remote Sensing to Hydrology* 28, 15–25.
809 [https://doi.org/10.1016/S1474-7065\(03\)00004-4](https://doi.org/10.1016/S1474-7065(03)00004-4)

810 Skidmore, A.K., Pettorelli, N., Coops, N.C., Geller, G.N., Hansen, M., Lucas, R., Múcher,
811 C.A., O'Connor, B., Paganini, M., Pereira, H.M., Schaepman, M.E., Turner, W.,
812 Wang, T., Wegmann, M., 2015. Environmental science: Agree on biodiversity metrics
813 to track from space. *Nat. News* 523, 403. <https://doi.org/10.1038/523403a>

814 Szantoi, Z., Escobedo, F., Abd-Elrahman, A., Smith, S., Pearlstine, L., 2013. Analyzing fine-
815 scale wetland composition using high resolution imagery and texture features. *Int. J.*
816 *Appl. Earth Obs. Geoinformation* 23, 204–212.
817 <https://doi.org/10.1016/j.jag.2013.01.003>

818 Teillet, P.M., Fedosejevs, G., Thome, K.J., Barker, J.L., 2007. Impacts of spectral band
819 difference effects on radiometric cross-calibration between satellite sensors in the
820 solar-reflective spectral domain. *Remote Sens. Environ.* 110, 393–409.
821 <https://doi.org/10.1016/j.rse.2007.03.003>

822 Tilman, D., Clark, M., Williams, D.R., Kimmel, K., Polasky, S., Packer, C., 2017. Future
823 threats to biodiversity and pathways to their prevention. *Nature* 546, 73.
824 <https://doi.org/10.1038/nature22900>

825 Todd, M.J., Muneeppeerakul, R., Pumo, D., Azaele, S., Miralles-Wilhelm, F., Rinaldo, A.,
826 Rodriguez-Iturbe, I., 2010. Hydrological drivers of wetland vegetation community
827 distribution within Everglades National Park, Florida. *Adv. Water Resour., Special*
828 *Issue on Novel Insights in Hydrological Modelling* 33, 1279–1289.
829 <https://doi.org/10.1016/j.advwatres.2010.04.003>

830 Tomaselli, V., Adamo, M., Veronico, G., Sciandrello, S., Tarantino, C., Dimopoulos, P.,
831 Medagli, P., Nagendra, H., Blonda, P., 2017. Definition and application of expert
832 knowledge on vegetation pattern, phenology, and seasonality for habitat mapping, as
833 exemplified in a Mediterranean coastal site. *Plant Biosyst. - Int. J. Deal. Asp. Plant*
834 *Biol.* 151, 887–899. <https://doi.org/10.1080/11263504.2016.1231143>

835 Tompkins, S., Mustard, J.F., Pieters, C.M., Forsyth, D.W., 1997. Optimization of
836 endmembers for spectral mixture analysis. *Remote Sens. Environ.* 59, 472–489.
837 [https://doi.org/10.1016/S0034-4257\(96\)00122-8](https://doi.org/10.1016/S0034-4257(96)00122-8)

838 Tuia, D., Persello, C., Bruzzone, L., 2016. Domain adaptation for the classification of remote
839 sensing data: an overview of recent advances. *IEEE Geosci. Remote Sens. Mag.* 4,
840 41–57. <https://doi.org/10.1109/MGRS.2016.2548504>

841 Tuxen, K., Kelly, M., 2008. Multi-scale functional mapping of tidal marsh vegetation using
842 object-based image analysis, in: Blaschke, T., Lang, S., Hay, G.J. (Eds.), *Object-*

843 Based Image Analysis: Spatial Concepts for Knowledge-Driven Remote Sensing
844 Applications, Lecture Notes in Geoinformation and Cartography. Springer Berlin
845 Heidelberg, Berlin, Heidelberg, pp. 415–442. [https://doi.org/10.1007/978-3-540-](https://doi.org/10.1007/978-3-540-77058-9_23)
846 [77058-9_23](https://doi.org/10.1007/978-3-540-77058-9_23)

847 Walker, L.R., Smith, S.D., 1997. Impacts of Invasive Plants on Community and Ecosystem
848 Properties, in: Luken, J.O., Thieret, J.W. (Eds.), Assessment and Management of
849 Plant Invasions, Springer Series on Environmental Management. Springer New York,
850 New York, NY, pp. 69–86. https://doi.org/10.1007/978-1-4612-1926-2_7

851 Wang, C., Menenti, M., Stoll, M.-P., Belluco, E., Marani, M., 2007. Mapping mixed vegetation
852 communities in salt marshes using airborne spectral data. Remote Sens. Environ.
853 107, 559–570. <https://doi.org/10.1016/j.rse.2006.10.007>

854 Wang, L., Dronova, I., Gong, P., Yang, W., Li, Y., Liu, Q., 2012. A new time series
855 vegetation–water index of phenological–hydrological trait across species and
856 functional types for Poyang Lake wetland ecosystem. Remote Sens. Environ. 125,
857 49–63. <https://doi.org/10.1016/j.rse.2012.07.003>

858 Xie, Q., Dash, J., Huang, W., Peng, D., Qin, Q., Mortimer, H., Casa, R., Pignatti, S., Laneve,
859 G., Pascucci, S., Dong, Y., Ye, H., 2018. Vegetation Indices Combining the Red and
860 Red-Edge Spectral Information for Leaf Area Index Retrieval. IEEE J. Sel. Top. Appl.
861 Earth Obs. Remote Sens. 11, 1482–1493.
862 <https://doi.org/10.1109/JSTARS.2018.2813281>

863 Yang, X., 2007. Integrated use of remote sensing and geographic information systems in
864 riparian vegetation delineation and mapping. Int. J. Remote Sens. 28, 353–370.
865 <https://doi.org/10.1080/01431160600726763>

866 Zhang, J., Okin, G.S., Zhou, B., 2019. Assimilating optical satellite remote sensing images
867 and field data to predict surface indicators in the Western U.S.: Assessing error in
868 satellite predictions based on large geographical datasets with the use of machine
869 learning. Remote Sens. Environ. 233, 111382.
870 <https://doi.org/10.1016/j.rse.2019.111382>

871 Zhao, W., Du, S., 2016. Learning multiscale and deep representations for classifying
872 remotely sensed imagery. ISPRS J. Photogramm. Remote Sens. 113, 155–165.
873 <https://doi.org/10.1016/j.isprsjprs.2016.01.004>

874 Zlinszky, A., Schroiff, A., Kania, A., Deák, B., Mücke, W., Vári, Á., Székely, B., Pfeifer, N.,
875 2014. Categorizing Grassland Vegetation with Full-Waveform Airborne Laser
876 Scanning: A Feasibility Study for Detecting Natura 2000 Habitat Types. Remote
877 Sens. 6, 8056–8087. <https://doi.org/10.3390/rs6098056>

879 **Figure captions**

880 Fig. 1: (left) Location of the Sougéal marsh study site on the Mont-Saint-Michel Bay Natura
 881 2000 site and (right) locations of floristic surveys in 2017 and 2018 on the orthophotograph
 882 acquired by UAV on 18 May 2018.

883 Fig. 2: Spectral (band width) and spatial features of Sentinel-2, Pleiades and Sequoia (UAV)
 884 sensors.

885 Fig. 3: The general processing workflow composed by four steps. 1) Unsupervised
 886 classification of floristic data. 2) Supervised classification of multirate UAV data to provide a
 887 reference map. 3) Estimation of habitats' abundances using spectral unmixing with two
 888 cases: A) extraction of endmembers in UAV imagery; and B) extraction of endmembers in
 889 satellite imagery. 4) accuracy assessment.

890 Fig. 4: Impact of spatial resolution on the spectral response of survey areas. a) Sentinel-2
 891 resolution (10m) ; b) Pleiades resolution (2m) ; c) UAV resolution (0.2m) ; d) Example of
 892 plant communities distribution.

893 Fig. 5: Topography and plant communities of the Sougeal marsh. Left: digital surface model
 894 derived from UAV RGB data. Right: color composite of wet grasslands plant communities in
 895 the Sougeal marsh derived from RF classification of UAV imagery. Specific areas: a)
 896 ecotone; b) MH on small dikes of channels; c) hygrophilic depression. Classes description: M
 897 – Mesophilic; MH – Meso-Hygrophilic; H – Hygrophilic.

898 Fig. 6: Color composites of wet grasslands plant communities in the Sougeal marsh derived
 899 from spectral unmixing of a) nov-pl-sat, b) nov-pl-uav, c) apr-s2-sat, d) apr-s2-uav, e) may-
 900 s2-sat, f) may-s2-uav, g) may-pl-sat, and h) may-pl-uav. Classes description: M – Mesophilic;
 901 MH – Meso-Hygrophilic; H – Hygrophilic.

902 Fig. 7: Fuzzy producer's (PA_f) and user's (UA_f) accuracy per classes and unmixing
 903 processes. Classes description: M – Mesophilic; MH – Meso-Hygrophilic; H – Hygrophilic; BS
 904 - Bare soils; Ud – *Urtica dioica* and W – Water. PA: Producer's accuracy, UA: User's

905 accuracy.

906 Fig. 8: Scatter plots of UAV versus Satellite measurements with (red) and without (blue) DA
907 for the NIR spectral band: a) Pleiades at 2017-11-06; b) Pleiades at 2018-05-20; c) Sentinel-
908 2 at 2018-04-19 ; and d) Sentinel-2 at 2018-05-19.